

Comparisons of polycarbonate and polycarbonate/carbon nanotube nanocomposites and their microcellular foams prepared using supercritical carbon dioxide

Sun-Mou Lai · Ruey-Chi Hsu · Chi-Yuan Hsieh · Fang-Chyou Chiu

Received: 14 October 2014 / Accepted: 13 December 2014 / Published online: 24 December 2014
© Springer Science+Business Media New York 2014

Abstract Polycarbonate (PC)/multi-walled carbon nanotube (CNT) nanocomposites were prepared using a Haake internal mixer. The neat PC and nanocomposites were further soaked under supercritical CO₂ (scCO₂) atmosphere for various periods to develop microcellular foams. Morphological results confirmed the fine dispersion of CNTs in the composites, resulting in superior thermal stability (44 °C increase at 5 wt% loss) and dynamic storage modulus (22 % increase at 75 °C) compared with the neat PC. The composites exhibited a rheological percolation threshold at 2 wt% CNT loading. The microcellular structure of foamed samples revealed that longer soaking periods (≤ 2 h) in scCO₂ resulted in larger cell sizes, and higher CNT loadings caused higher cell densities at similar soaking periods. Foaming-induced PC crystals were verified through differential scanning calorimetry and X-ray diffraction. More crystals (up to 38 %) were developed with increasing soaking time. The added CNT facilitated the crystallization of PC and obtained crystals with higher stability. The two-melting phenomenon exhibited by the foams represented the melting of the originally less-stable crystals and heating-annealed crystals. The neat PC foams or low CNT-loaded composite foams demonstrated improved thermal stability compared with their unfoamed counterparts.

Introduction

Thermally insulated products exhibit the advantage of energy conservation by reducing heat conduction, convection, and radiation. Thus, microcellular polymeric foams have received much attention in the emerging energy concern caused by the depletion of fossil fuel energy resources. Conventional isopentane or dichlorodifluoromethane are used as physical blowing agents to produce foamed products. However, these blowing agents potentially destroy the ozone layers and/or produce global warming effects, which are detrimental to our ecosystems. The use of eco-friendly foaming agents, such as supercritical carbon dioxide (scCO₂) and water, is increasing. In particular, polymer foaming using scCO₂ ($T_c = 31$ °C, $P_c = 7.38$ MPa) can produce fine cellular structures at relatively low CO₂ content. Various polymers, such as polyethylene [1], polypropylene [2], poly(ethylene terephthalate) [3], polystyrene [4–6], poly(lactic acid) [7], and polycarbonate (PC) [8–10] have been evaluated to prepare microcellular foams using scCO₂.

In addition to conventional foaming polymers, using nanoparticles to enhance the performance of foamed materials has been pursued [11, 12]. Few studies have been conducted on PC-based nanocomposite foams [13–16]. Hu et al. [14] reported that nanoclay can function as an efficient cell-nucleating agent in scCO₂-foamed PC systems to enhance the crystallization of PC. With the addition of nanoclay, the induction time of crystallization decreases and the crystallization rate increases. Zhai et al. [15] indicated that adding nanosilica could result in more uniform cell size distribution of PC/silica nanocomposite foams than that of the neat PC foam by significantly reducing the energy barrier for heterogeneous cell nucleation. In addition to nanoclay and nanosilica, conductive

S.-M. Lai
Department of Chemical and Materials Engineering, National I-Lan University, I-Lan 260, Taiwan, ROC

R.-C. Hsu · C.-Y. Hsieh · F.-C. Chiu (✉)
Department of Chemical and Materials Engineering, Chang Gung University, Taoyuan 333, Taiwan, ROC
e-mail: maxson@mail.cgu.edu.tw

carbon nanotubes (CNTs) can function as ideal nanofillers for PC-based nanocomposites. CNTs possess excellent properties, including high electrical conductivity, low density, tremendous mechanical strength, and excellent flexibility [17]. Incorporating CNTs to achieve PC-based nanocomposites with enhanced electrical conductivity and mechanical properties has been well recognized [18–20]. However, to our best knowledge, PC/CNT nanocomposite foams are lack of comprehensive investigation. Monnereau et al. [21] recently reported that the efficient foaming of PC/CNT nanocomposites occurred when low saturation pressure of scCO₂ was applied. No expansion of the samples was observed at high pressure of scCO₂. The great ability of prepared foams with low CNT loadings to absorb electromagnetic radiation was demonstrated as well. However, no detailed thermal (crystalline) properties were discussed. From academic and practical viewpoints, the effects of CNT loading and soaking period under scCO₂ on the resulting cellular structure and thermal properties of PC/CNT nanocomposite foams merit further investigation. As mentioned above, the combination of PC and CNT resulted in a material exhibiting electrical conductive properties with a high modulus and improved heat resistance. Foaming of the PC/CNT nanocomposites can be further valuable for some applications, such as in structural electromagnetic interference shielding devices, electrostatic painting of lightweight materials, and thermally insulating lightweight component for auto applications.

In the present study, we aim to investigate the differences in the structure and physical properties of PC and PC/CNT nanocomposite foams and explore the role of CNTs in scCO₂ foaming of PC. Considering that nanoparticles promote heterogeneous cell nucleation during foaming, we added different amounts of CNTs in the PC matrix through conventional melt mixing. The thermal stability and the dynamic mechanical and rheological properties of the prepared PC/CNT nanocomposites were analyzed and compared with those of the neat PC. The cellular morphologies, crystalline characteristics, and thermal stabilities of the PC and nanocomposite foams prepared with scCO₂ as the physical blow agent were also investigated. The effects of CNT loading and soaking time in scCO₂ on the complex melting behavior of the prepared foams were highlighted.

Experimental

Materials

PC with average molecular weight of 22500 g/mol and melt flow index of 30 g/min (ASTM D1238) was purchased from LG-Dow Co. Multi-walled CNTs were

manufactured by Mitsui Co., Japan and were directly used as received. According to the supplier, the CNTs possess a carbon purity of >99 %, minimum length of 10 μm, and diameter of 40–90 nm. Industrial-grade CO₂ was supplied by Shinn Hwa Gas Co., Taiwan and was used to produce scCO₂ for preparing foamy materials.

Preparation of samples

PC and CNTs were pre-dried in a vacuum oven at 60 °C for 24 h, and then fed into an internal mixer (Haake Polydriver) for mixing at 60 rpm and 250 °C for 8 min. CNT loadings in the PC matrix varied at 0.3, 0.6, 1, 1.5, 2, and 3 wt% and designated with CNT-filled composite codes of PC-03, PC-06, PC-1, PC-1.5, PC-2, and PC-3, respectively. For comparison, neat PC was melt processed at the same condition. The prepared composites and PC were compression molded at 250 °C to form 1-mm-thick disks with 2-cm diameter for foaming experiments. The disks were first placed in a steel vessel equipped with a heating jacket and a temperature controller. The vessel was then flushed with CO₂ by connecting to a CO₂ cylinder. Saturation (soaking) pressure of CO₂ was adjusted at ca. 19.3 MPa (2800 psi), and the temperature was maintained at 100 °C. The polymer disks were soaked in the vessel under scCO₂ atmosphere for various time periods (i.e., 0.5, 1, 2, and 4 h). Subsequently, the saturation pressure was rapidly released (within 3 s) to induce phase instability for cells (bubbles) nucleation and growth. This pressure-induced phase separation caused the development of foamy samples. After depressurization, the vessel was opened to cool the samples and obtain the stabilized cellular structure. The code for the individual composite foams is “composite code-X”, where X represents the soaking hour under scCO₂. For instance, PC-06-05 denotes the PC-06 composite soaked for 0.5 h and PC-2-4 represents 4-h-soaked PC-2 composite. For the neat PC foam, the code is PC-0-X and 2-h-soaked neat PC is coded as PC-0-2.

Characterization

To evaluate the CNT dispersibility within the PC matrix and the cellular structure of foamed samples, we elucidated the morphology of the cryo-fractured (in liquid nitrogen) surfaces of the specimens with or without foaming using a scanning electron microscope (SEM, Hitachi S-3000 N). The ultrathin sections (<90 nm) of the cryo-microtomed composite films were evaluated using a transmission electron microscope (TEM, JEOL JEM 1230) to confirm the dispersion status of CNTs within the PC matrix.

Crystalline characteristics (melting behavior) of foamed samples were evaluated using a differential scanning calorimeter (DSC Q10) and scanned from room temperature

to 250 °C. A Siemens D5005 X-ray unit operating at 40 kV and 40 mA was used in XRD experiments to evaluate the crystalline structure of the prepared foams. The X-ray source was CuK α radiation with a wavelength of 1.54 Å. The thermal stabilities of foamed/unfoamed samples were measured using a thermogravimetric analyzer (TGA, TA Q50) under an air environment. The heating process was conducted from room temperature to 700 °C at 20 °C/min. The rheological properties of unfoamed samples were determined using an Anton Paar-Physica MCR 101 rheometer with a parallel plate fixture of 20-mm diameter and 1-mm gap. The samples were maintained between the preheated plates at 250 °C for ca. four minutes prior to measurement. Strain amplitude was set within the linear viscoelastic regime of 1 % [22], and sweep frequency varied from 0.01 to 100 rad/s. The dynamic mechanical properties of the rectangular thin-film specimens were measured using a TA DMA 2980 system. The measurements were carried out in tension mode at 2 °C/min heating rate and frequency of 1 Hz in air. The density of neat PC and foamed samples was measured using an A&D GR-200 analytical balance.

Results and discussion

Comparison of PC and PC/CNT nanocomposites

Dispersibility of CNT

Figure 1 shows the SEM images of the unfoamed PC/CNT composites with different CNT loadings. CNTs were randomly and homogeneously dispersed throughout the PC matrix in all samples. The result could be attributed to the possible π - π electron interaction between the C=C on the CNT surfaces and in the phenylene rings of PC, as well as the efficient mixing process. At a low CNT loading (i.e., 0.3 %), the individual nanotubes without a developing network structure was clearly detected. As the CNT loading increased to 2 and 3 %, the network of the nanotubes was evidently observed. The insets of Fig. 1c, d present the corresponding TEM images of the composites. The morphology of the finely dispersed CNTs was also observed. The dispersibility of CNT confirmed that PC/CNT nanocomposites with various CNT loadings were obtained, which is consistent with previous results [19, 20]. The fine dispersion of nanoparticles is important to develop uniform cell size in nanocomposite foams [15].

Rheological properties

In addition to the morphological observations, the dispersion and interconnectivity of CNTs within the polymer

matrix were revealed from rheological property measurements. Figure 2a illustrates the results of complex viscosity (η^*) versus angular frequency (ω) of the samples, in which η^* increased as the CNT loading increased in the samples. Remarkably, η^* exhibited an evidently non-Newtonian behavior at low frequencies when CNT loadings were 2 and 3 % (cf. PC-2 and PC-3, respectively). This pseudo-solid-like response suggested that CNTs developed a percolated network structure [23, 24]. In addition to the complex viscosity, storage modulus (G') was also measured, as shown in Fig. 2b. An increase in G' was noted with the increasing CNT loading and frequency. PC-2 and PC-3 showed evidently higher G' values than those of the other samples within the low-frequency region ($\omega < 1$). The slope of the G' data within the low-frequency region was more flattened in PC-2 and PC-3 than those in the other samples. The apparent G' alterations in the two samples were ascribed to the CNT network structure formation. The inset of Fig. 2b depicts the increase in the G' values with the increasing CNT loading in the samples at $\omega = 0.01$ rad/s. The abrupt increase in G' at 2 % CNT loading verified the rheological percolation threshold of PC/CNT nanocomposites. These rheological results were in agreement with the morphological observations. The percolation threshold value of our PC/CNT nanocomposites is similar to the value reported by Potschke et al. [25] but higher than that reported by Lin et al. [26]. The differences in the preparation methods of the nanocomposites and the aspect ratio/purity of CNTs account for the discrepancies in the results.

Thermal stability and dynamic mechanical properties

The thermal degradation behavior of the neat PC and its nanocomposites is presented in Fig. 3a based on the TGA data. A typical multi-staged degradation of the PC matrix in air was observed [27], and the degradation temperature shifted to higher temperatures as the CNT loading increased in the samples. The temperature at 5 wt% loss (T_5 %) increased from 448 °C for the neat PC to 492 °C for the PC-3 nanocomposite. The increase in degradation temperature was attributed to the combined effects of superior thermal stability and ability of the scavenging free radicals of the well-dispersed CNTs, thus forming the protective layers in the PC matrix during heating. The representative thermal stability data (T_5 % and T_{50} %) of the samples are summarized in Table 1.

The mechanical properties of the neat PC and its composites were compared through DMA. Figure 3b depicts the temperature-dependent storage modulus (E') of the representative samples. The neat PC and composites exhibited similar decreasing E' trends with the increasing temperature; the E' followed the order of PC-3 > PC-

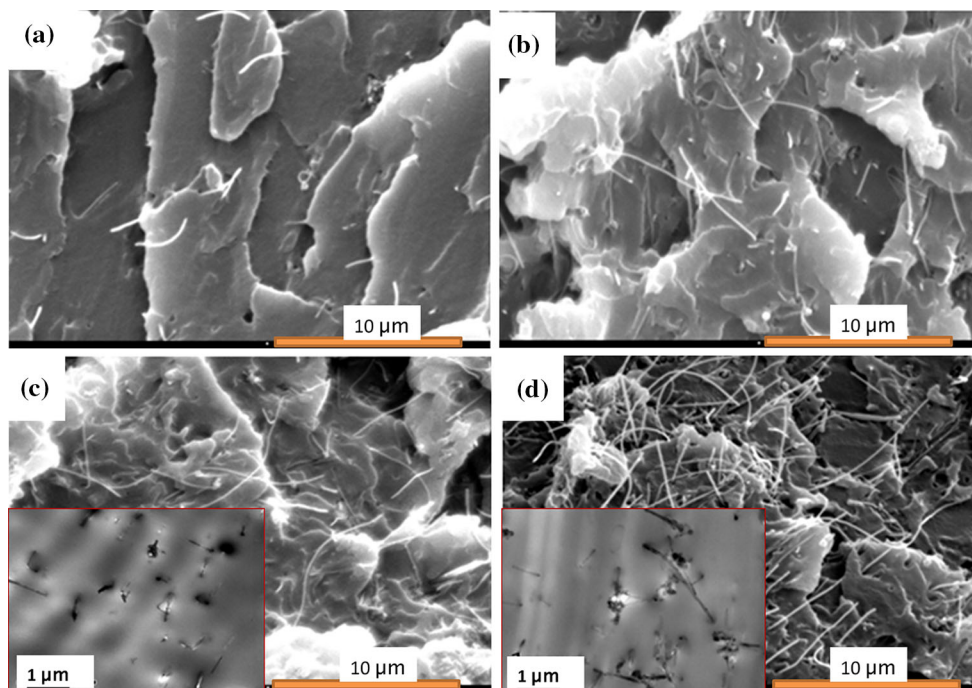


Fig. 1 SEM images of PC/CNT nanocomposites: **a** PC-03, **b** PC-1, **c** PC-2, and **d** PC-3. *Insets* TEM images of the corresponding nanocomposites

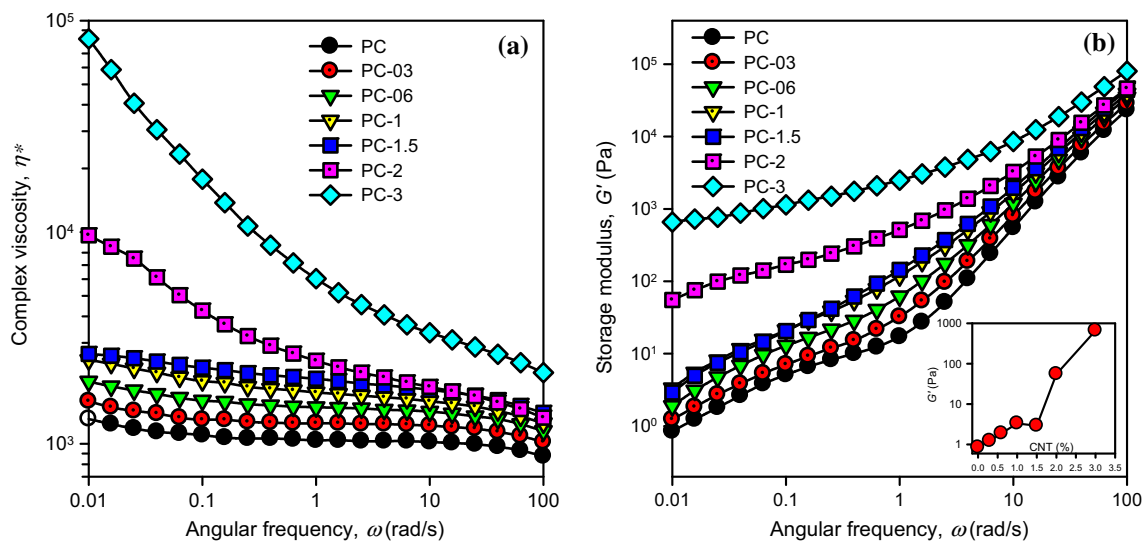


Fig. 2 Rheological properties of unfoamed samples: **a** complex viscosity versus frequency, and **b** storage modulus versus frequency (*inset*: storage modulus at $\omega = 0.01$ rad/s as a function of CNT loading)

1 > neat PC at similar temperatures. The E' value at 30 °C increased from 2.27 GPa for the neat PC to 2.45 GPa for PC-1 and then further increased to 2.62 GPa (~ 15 % increase) for PC-3. The increase was more evident at 75 °C; that is, 2.05 GPa for the neat PC and 2.51 GPa (~ 22 % increase) for PC-3. Thus, the stiffness of the neat PC added with CNTs was evidently enhanced. The abrupt decrease in E' within 140 °C demonstrated the glass

transition of PC. The inset of Fig. 3b shows the loss tangent ($\tan \delta$) versus the temperature of the samples. The composites exhibited lower $\tan \delta$ peak heights than the neat PC. Higher CNT loadings resulted in lower peak heights. These results indicated that the composites with rigid CNTs exhibited more elastic characteristics. The T_g determined from the location of $\tan \delta$ peak showed a negligible increase (ca. 1 °C) when added with CNT.

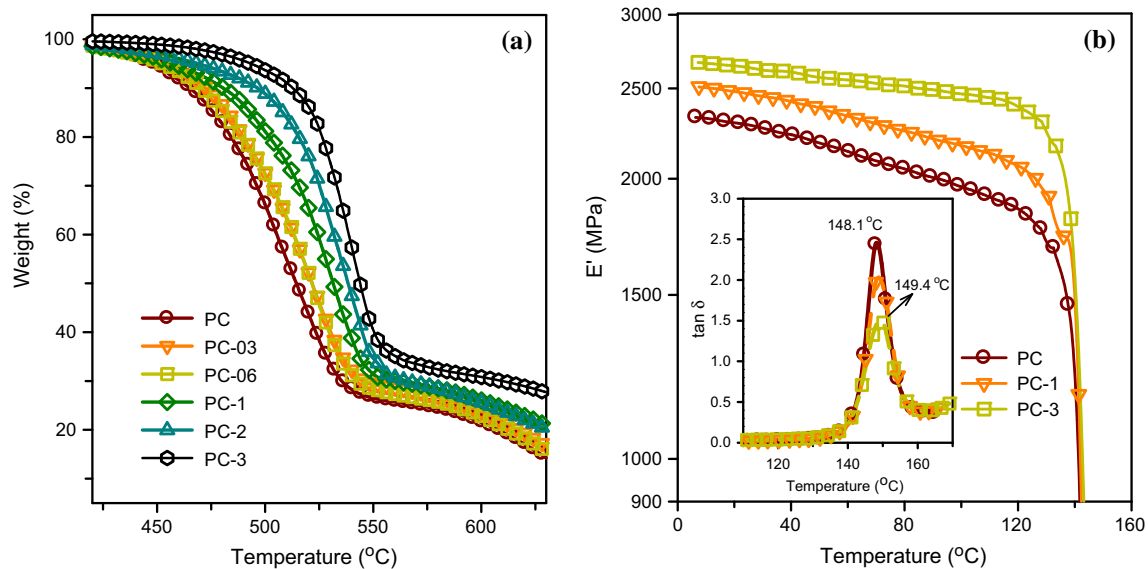


Fig. 3 **a** TGA-scanned curves in air, and **b** DMA storage modulus versus temperature (*inset*: loss tangent vs. temperature) of unfoamed samples

Table 1 Representative TGA data of samples scanned in air

Samples	neat PC	PC-03	PC-06	PC-1	PC-2	PC-3
T ₅ % (°C)	448	451	454	456	468	492
T ₅₀ % (°C)	514	522	524	531	538	544

Comparison of PC and nanocomposite foams

Microcellular structure

After confirming the uniform dispersion of CNTs throughout the PC matrix, Fig. 4 shows the SEM images of the fractured surfaces of the neat PC foams soaked in scCO₂ for various periods. The microcellular cells with average size <3 μm was observed for the prepared foams. It is also noted that longer soaking periods (0.5–2 h) resulted in larger cell sizes. Without nanoparticle incorporation, the foaming process basically prevailed in the homogeneous nucleation process. Longer soaking periods increased the solubility and concentration of scCO₂ in the PC matrix. Therefore, higher foaming efficiencies tended to occur, which accounted for the larger cell sizes with the increasing soaking periods. However, cell rupture was observed after a long soaking period of 4 h (Fig. 4d). This broken cellular structure indicated the overgrowth of cells (bubbles) caused by the high scCO₂ concentration entrapped within the PC matrix. The images with higher magnification are shown in the inset of the individual figures. The microcellular structure with the apparent “veins (dense bands)” surrounding the cells was also detected. The “veins” (arrowed) were presumed to be formed by the

strain-induced crystallization (crystalline lamellae) of PC during expansion process of foaming, which is similar to those observed on the surface of the bubbles of PC foams [28].

For the soaking time-dependent cellular structure of nanocomposite foams, the SEM images of 1 % CNT-added samples (PC-1-X) are presented in Fig. 5. Other composite foams exhibited similar trend (data not shown for brevity). The images revealed that the cell size basically increased with the soaking period, which was similar to the observation in the neat PC foams (Fig. 4). The effect of CNT loading on the growth of microcellular structure is demonstrated by the SEM images in Fig. 6. The representative 0.5 h-soaked foams were selected for investigation. The foam with higher CNT loading demonstrated more cells and displayed cells with less-rounded shape. The average cell size and the cell density of the selected foams calculated according to the following equation [29] are listed in Table 2.

$$N = (n \cdot M^2 / A)^{3/2}, \quad (1)$$

where N is the cell density, n represents the number of cells (bubbles), M is the magnification factor, and A is the area of the SEM image. Generally, cell size and cell density increased with prolonged soaking periods for the neat PC foams and nanocomposites foams. The 2-h-soaked nanocomposite foams possessed the cells with higher density and smaller size than those of neat PC foam. These findings resulted from the combined effects of CNT-induced cell nucleation and CNT-enhanced rigidity of composite matrix (networking capability). Chen [29] attributed the high foaming efficiency of CNT-filled samples to the high

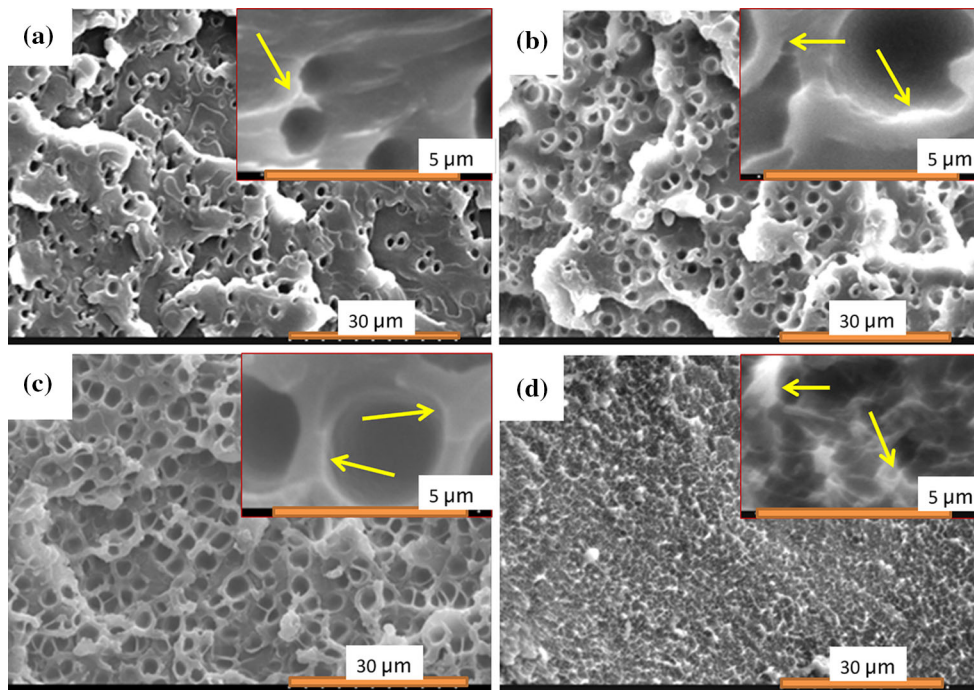


Fig. 4 SEM images of the microcellular structures of the neat PC foams: **a** 0.5-, **b** 1-, **c** 2-, and **d** 4-h soaking periods. *Insets* a higher magnification for individual foams

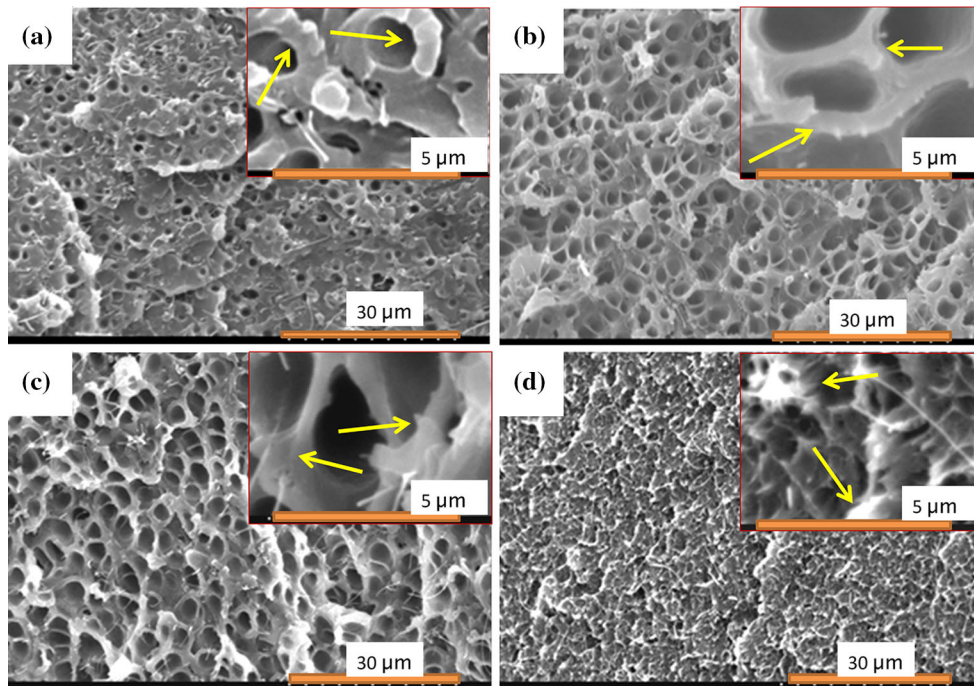


Fig. 5 SEM images of the microcellular structures of the PC-1-X foams: **a** 0.5-, **b** 1-, **c** 2-, and **d** 4-h soaking periods. *Insets* a higher magnification for individual foams

aspect ratio of CNTs, which exhibit an important role in heterogeneous nucleated foaming. In the present system, CNTs also promoted the scCO₂ foaming efficiency (circled

in Fig. 6), thus decreasing the energy barrier for cell nucleation. The density of neat PC and selected foams was also measured. The neat PC possesses a density of

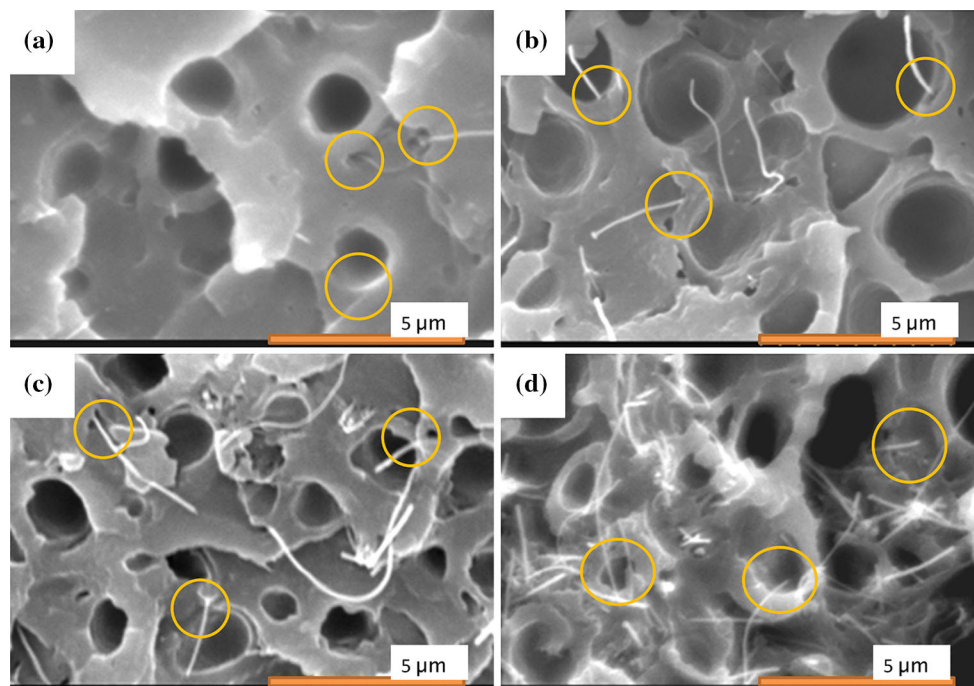


Fig. 6 SEM images of the microcellular structures of: **a** PC-03-05, **b** PC-06-05, **c** PC-1-05, and **d** PC-3-05

Table 2 Average cell size, cell density, and foam density of representative foams

Samples	PC-0-05	PC-0-2	PC-03-05	PC-03-2	PC-2-05	PC-2-2	PC-3-05	PC-3-2
Size (μm) ^a	1.47	2.31	1.62	2.07	1.96	2.09	1.61	1.79
Cell density ^b	0.86	1.41	1.02	1.98	1.62	2.04	1.92	2.46
Foam density ^c	0.934	0.874	0.897	0.866	0.944	0.877	0.959	0.835

^a Standard deviation ca. <30 %

^b Unit: $\text{cell}/\text{cm}^3 (\times 10^{10})$

^c Unit: g/cm^3

1.19 g/cm^3 and the foams show lower density values as compared in Table 2. The density decreased with increasing the soaking time from 0.5 to 2 h for the samples having the identical CNT loading, which is ascribed to the higher forming efficiency of a longer soaking time. Despite the cell density increased with increasing CNT loading, the effect of CNT loading amount on the foams' density did not show a simple trend. Both factors of the higher density of CNT compared to the neat PC and the higher crystallinity developed with a higher CNT loading through an identical soaking time (see the following section) should be considered for the observation. More systematic study is required to reveal the effect of foaming-induced crystallinity on the density of resultant foams.

Crystalline characteristics

To determine the effects of foaming and CNT additions on the thermal (melting) behavior of the samples, we scanned

the PC and nanocomposite foams using DSC under heating processes. Figure 7a illustrates the 20 °C/min-heated DSC thermograms of the neat PC foam and the selected composite foams soaked in scCO_2 for 0.5 h. A glass transition temperature of approximately 150 °C was observed for individual samples. PC-1-05 and PC-3-05 displayed slightly higher T_{gs} than those of the PC-0-05 and PC-03-05 samples, which could be attributed to the inhibition of the PC chain mobility by the well-dispersed CNTs. In addition to the glass transition, two shallow endothermic “peaks” were identified in each thermogram. The low-temperature “peak” (peak I) was located at approximately 185 °C, and the high-temperature “peak” (peak II) was detected at approximately 215 °C. These two peaks were not observed for the unfoamed PC and nanocomposites (data not shown). They were more evident for the composite foams than those of the neat PC foam. These peaks were associated with the melting of PC crystals [30, 31], which were grown during the scCO_2 foaming processes. As shown in

Fig. 7 20 °C/min-heated DSC thermograms of the selected foams after soaking in scCO₂ for **a** 0.5 h, **b** 1 h, **c** 2 h, and **d** 4 h

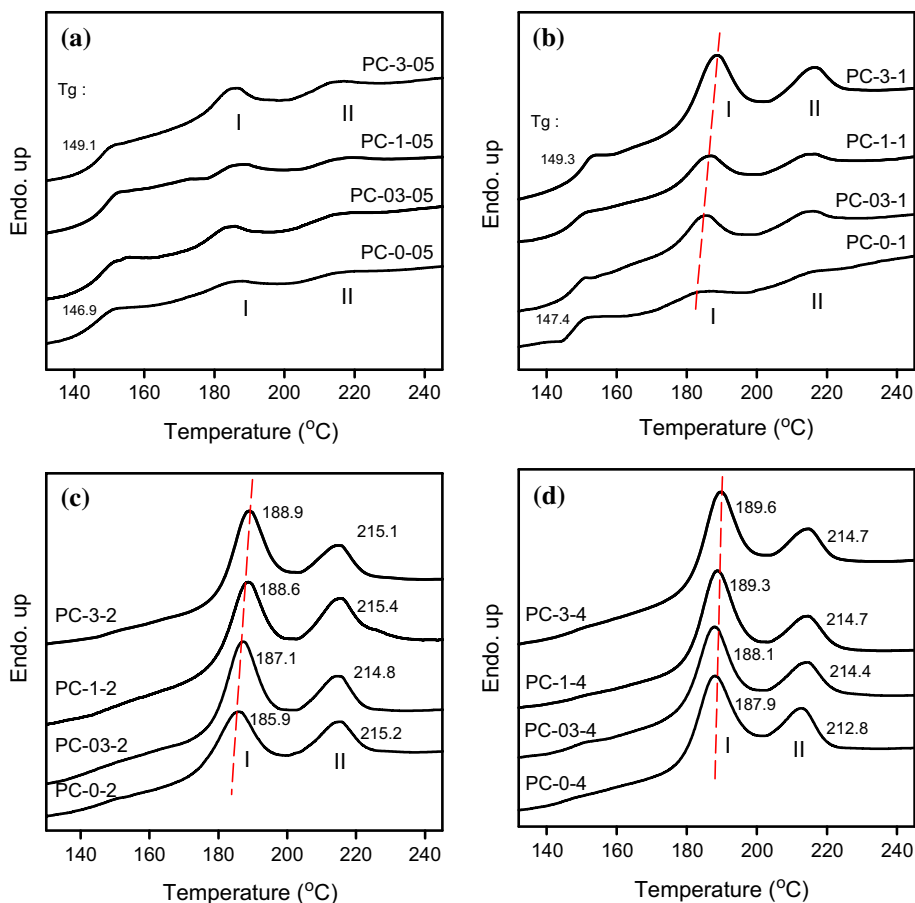


Fig. 7b, the two peaks became more intense for 1-h-soaked composite foams than those for their 0.5-h-soaked counterparts. Peak I shifted to higher temperatures with increasing CNT loading, whereas the position of peak II remained constant. Remarkably, the intensity of the peaks increased with the CNT loading; PC-3-1 exhibited the highest intensity. For the peaks of neat PC foam, they slightly increased when the soaking period was prolonged from 0.5 to 1 h. These results demonstrated that higher CNT loadings induced higher amount of PC crystals. CNT-induced heterogeneous cell nucleation played an important role for this result. The CNTs led to a more efficient foaming (expansion) process; hence, the alignment of the PC chains through similar soaking periods became more possible. Consequently, higher amounts of crystals were developed mainly during the expansion (depressurization) process. It is also believed that minor amount of crystals might have grown during the soaking process. Figure 7c, d show the thermograms of 2-h- and 4-h-soaked foams. The melting peaks were enhanced for all samples, particularly for the neat PC foam. The intensities of the peaks of the composite foams almost reached the plateau (maximum values) for the soaking period of 2 h. However, the neat PC

foam exhibited similar peak intensity at a longer time of 4 h. The evolution of the peak intensity with soaking time clearly implied that CNT addition facilitated the crystallization of the PC matrix foam. The temperatures of peaks I (T_{m1}) and II (T_{m2}) are listed in the figures. The result of the higher CNT loading resulted in higher T_{m1} value, which demonstrated that the presence of more CNTs could induce T_{m1} -associated crystals with higher stability. This result could be attributed to the optimal alignment of the PC chains within the crystals caused by the higher foaming efficiency. The increase in T_m with the increasing nanofillers' loading has been reported in other nanocomposite systems [23, 32]. This increase could also be ascribed to the decrease in the entropy change during the melting of crystals caused by the nanoconfined effect of the dispersed CNTs.

To further confirm the crystalline characteristics of the prepared foams, we conducted XRD experiments at room temperature. Figure 8a shows the XRD patterns of the neat PC and PC foams (cf. PC-0-2 and PC-0-4). The neat PC exhibited a broad amorphous halo around $2\theta = 17.2^\circ$, whereas the two foams showed an evident (020)/(-201) diffraction riding on the amorphous halo and a weak

(-222)/(303)/(223) diffraction around $2\theta = 25.6^\circ$ (monoclinic unit cell) [33]. The intensity of the peaks increased with the soaking time; hence, more crystals were developed (a higher crystallinity). This result corresponded to the observations regarding the DSC melting behavior. Crystallinity was estimated for the foamed samples based on the intensity of the individual amorphous and crystalline regions [34]. The values were ca. 28 % for PC-0-2 and 38 % for PC-0-4. The XRD patterns of PC-2, PC-2-2, and PC-2-4 are shown in Fig. 8b. The unfoamed PC-2 displayed amorphous feature, whereas the composite foams exhibited similar intensity of the crystalline diffractions. The crystallinity determined were ca. 33 and 36 % for PC-2-2 and PC-2-4, respectively. The comparable crystallinity values of the two foams implied that the crystallization of PC was nearly completed through the 2-h soaking process followed by the cells expansion. Further increasing the soaking time to 4 h resulted in slight increment in the crystallinity. In addition to the diffractions of PC crystals, a weak peak around $2\theta = 26.2^\circ$ was detected for the CNT-added samples. The additional diffraction represented the

interlayer spacing among the graphitic layer of the multi-walled CNTs. Figure 8c depicts the XRD patterns of the representative 4-h-soaked foams. The foams (including the neat PC foam) exhibited comparable diffraction intensities. This result implied that the inclusion of CNTs minimally altered the final crystallinity of the foams, whereas CNTs facilitated the growth rate of the PC crystals.

According to the XRD data, the two-melting peaks in DSC study should not be caused by different polymorphs. Four heating rates (4, 20, 40, and $80^\circ\text{C}/\text{min}$) were used in DSC analysis for the neat PC foams (Fig. 9a) to disclose the origin of the two-melting behavior. Two remarkable features could be observed in the figure. First, peak I shifted to higher temperatures with the increasing heating rate, whereas peak II moved to slightly lower temperatures. The two peaks partially overlapped when the heating rate was increased to 40 and $80^\circ\text{C}/\text{min}$. Second, the intensity ratio of peak II to peak I decreased as the heating rate increased. On the basis of these two observations, we speculated that the occurrence of crystals annealing during heating plays a major role for the two-melting behavior

Fig. 8 XRD patterns of **a** the neat PC and its foams, **b** PC-2 composite and its foams, and **c** 4-h-soaked selected foams

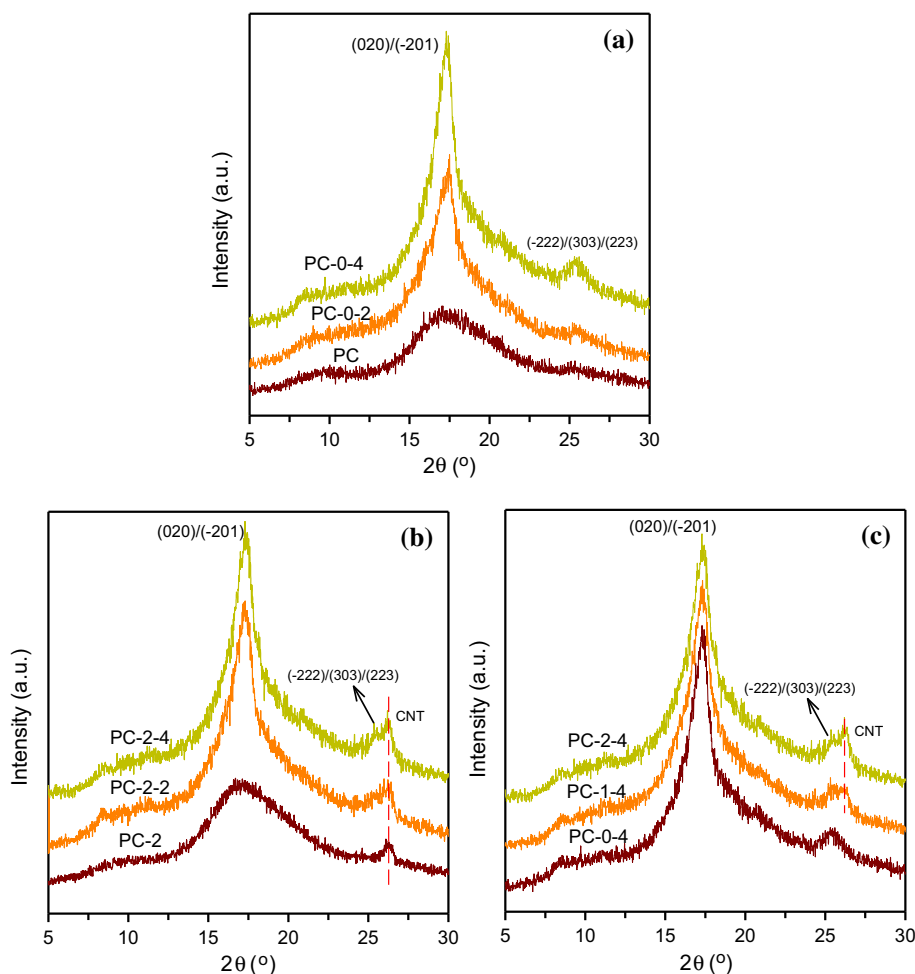
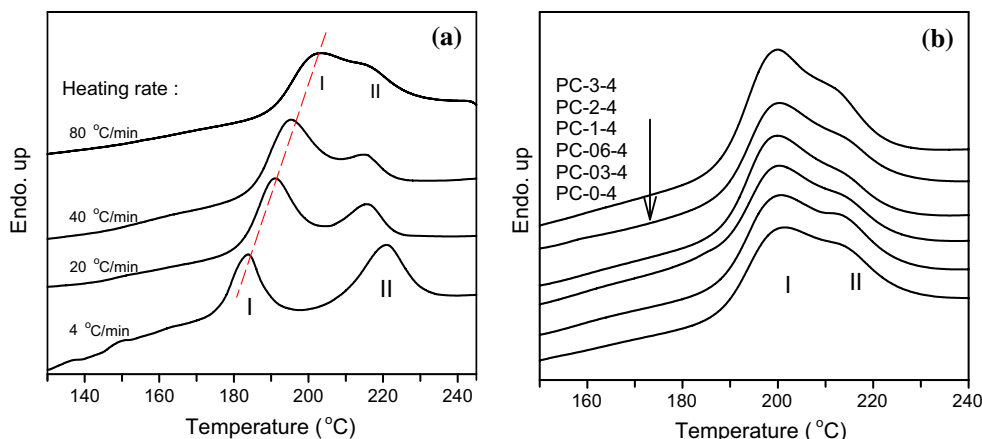


Fig. 9 DSC melting behavior of **a** the neat PC foam scanned under different rates, and **b** 80 °C/min-heated selected foams



[35]. Hence, the meltings comprised the originally formed less-stable crystals (peak I) and heating-annealed crystals (peak II). At a slower heating rate, higher amount of annealed crystals could be developed, resulting in relatively higher intensity of peak II. By contrast, a faster heating rate provided limited time (less opportunity) for annealing the crystals; thus, the intensity of peak II decreased or even appeared at a lower temperature. The shift of peak I with the heating rate was attributed to the superheating (thermal lag) effect. Figure 9b shows the 80 °C/min-heated DSC thermograms of 4-h-soaked foams. All samples, including the neat PC foam, evidently exhibited similar behavior of the peak I (at ca. 200 °C) that overlapped with the shoulder peak II. The apparent melting enthalpy of the overlapped peaks was measured for individual foams. The values (within the range of 23–25 J/g) were similar to one another, confirming that various foams exhibited similar crystallinity after 4-h soaking. The enthalpy values are transformed into crystallinity using 109.8 J/g [14] as the heat of fusion of 100 % crystallized PC. The crystallinity determined by DSC is around 22 % which is lower than those values measured based on XRD data. The DSC heating process-caused crystals annealing (or recrystallization) might be responsible for the different values obtained by the two methods.

Thermal stability

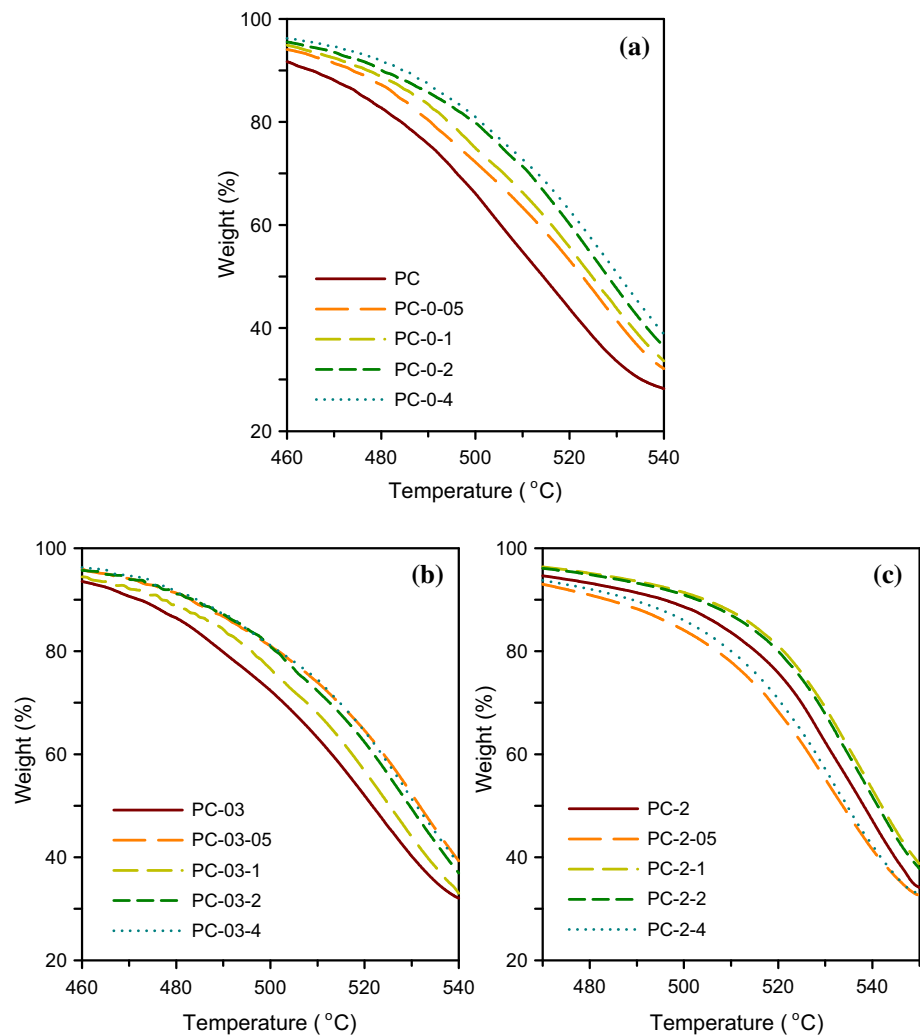
The advantage of adding CNTs on the improved thermal stability of PC is revealed in Fig. 3a. Figure 10a shows the TGA data of the neat PC and its foams. Increased thermal stability was observed in the PC foams compared to neat PC, and the foams showed slightly higher degradation temperatures with increasing soaking time. The thermal insulation feature of foamed samples was well known, which attributed to the enhanced thermal stability. However, the synergistic effect of adding CNTs and foaming

did not affect the representative composite foams, as observed in Fig. 10b, c. The thermal stability of the composite foams did not constantly increase with the increasing soaking time. At low CNT loadings (Fig. 10b), the PC-03-X foams showed improved thermal stability compared with the unfoamed PC-03; however, the improvement was not related to the soaking time. At higher CNT loadings (Fig. 10c), the improvement in thermal stability caused by the insulating effect deteriorated. This unexpected behavior was not previously reported. This phenomenon could be attributed to the effects of foaming on altering the dispersion status of CNTs and CNTs' high thermal conductivity (network formation), as well as to the thermal insulation effect of the cells.

Conclusions

PC/CNT nanocomposites were successfully fabricated via conventional melt mixing. Morphological observations revealed that CNTs were thoroughly dispersed in the PC matrix, confirming the affinity between the CNTs and PC. A rheological percolation threshold at a CNT loading of 2 wt% was determined for the composites. The nanocomposites showed improved thermal stability and stiffness compared with the neat PC; a higher CNT loading resulted in superior thermal stability and stiffness. The nanocomposites and neat PC were further soaked (saturated) under scCO₂ atmosphere for various periods to prepare foamy materials. The microcellular structure, including cell size and cell density, of the foams was characterized. The cell sizes increased with the soaking time, but the cells ruptured after 4-h soaking time. CNTs played a cell nucleation role in the foaming process, thus increasing the cell density. The final cell sizes accordingly decreased when CNTs were present in the foam. The foaming-induced (mainly during the expansion process) crystal growth of PC was also

Fig. 10 TGA-scanned curves of **a** the neat PC and its foams, **b** PC-03 and its foams, and **c** PC-2 and its foams



identified. The presence of CNTs in the foams facilitated the crystallization of PC and produced crystals with higher stability. The two-melting endotherms of the foams were attributed to the occurrence of crystals annealing during heating. Hence, these meltings comprised the originally formed crystals and the later annealed crystals. At higher CNT loadings in the composites, the improved foaming-stimulated thermal stability deteriorated.

References

- Cardoso ECL, Scagliusi SR, Parra DF, Lugão AB (2013) Gamma-irradiated cross-linked LDPE foams: characteristics and properties. *Radiat Phys Chem* 84:170–175
- Antunes M, Realinho V, Velasco JI (2010) Study of the influence of the pressure drop rate on the foaming behavior and dynamic-mechanical properties of CO₂ dissolution microcellular polypropylene foams. *J Cell Plast* 46:551–571
- Li D, Liu T, Zhao L, Yuan W (2012) Controlling sandwich-structure of PET microcellular foams using coupling of CO₂ diffusion and induced crystallization. *AIChE J* 58:2512–2523
- Chiu FC, Lai SM, Wong CM, Chang CH (2006) Properties of calcium carbonate filled and unfilled polystyrene foams prepared using supercritical carbon dioxide. *J Appl Polym Sci* 102: 2276–2284
- Yeh SK, Yang J, Chiou NR, Daniel T, Lee LJ (2010) Introducing water as a coblowing agent in the carbon dioxide extrusion foaming process for polystyrene thermal insulation foams. *Polym Eng Sci* 50:1577–1584
- Zhang C, Zhu B, Li D, Lee LJ (2012) Extruded polystyrene foams with bimodal cell morphology. *Polymer* 53:2435–2442
- Rouholamin D, Smith PJ, Ghassemieh E (2013) Control of morphological properties of porous biodegradable scaffolds processed by supercritical CO₂ foaming. *J Mater Sci* 48:3254–3263. doi:10.1007/s10853-012-7109-4
- Wong A, Leung SN, GaYG Li, Park CB (2007) Role of processing temperature in polystyrene and polycarbonate foaming with carbon dioxide. *Ind Eng Chem Res* 46:7107–7116
- Gong P, Taniguchi T, Ohshima M (2014) Nanoporous structure of the cell walls of polycarbonate foams. *J Mater Sci* 49: 2605–2617. doi:10.1007/s10853-013-7959-4

10. Ma Z, Zhang G, Yang Q, Shi X, Shi A (2014) Fabrication of microcellular polycarbonate foams with unimodal or bimodal cell-size distributions using supercritical carbon dioxide as a blowing agent. *J Cell Plast* 50:55–79
11. Antunes M, Velasco JI (2014) Multifunctional polymer foams with carbon nanoparticles. *Prog Polym Sci* 39:486–509
12. Ding J, Ma W, Song F, Zong Q (2013) Effect of nano-calcium carbonate on microcellular foaming of polypropylene. *J Mater Sci* 48:2504–2511. doi:10.1007/s10853-012-7039-1
13. Ito Y, Yamashita M, Okamoto M (2006) Foam processing and cellular structure of polycarbonate-based nanocomposites. *Macromol Mater Eng* 291:773–783
14. Hu X, Lesser AJ (2004) Enhanced crystallization of bisphenol-A polycarbonate by nano-scale clays in the presence of supercritical carbon dioxide. *Polymer* 45:2333–2340
15. Zhai W, Yu J, Wu L, Ma W, He J (2006) Heterogeneous nucleation uniformizing cell size distribution in microcellular nanocomposites foams. *Polymer* 47:7580–7589
16. Gedler G, Antunes M, Velasco JI (2013) Graphene-induced crystallinity of bisphenol A polycarbonate in the presence of supercritical carbon dioxide. *Polymer* 54:6389–6398
17. Yu MF, Lourie O, Dyer MJ, Monoli KM, Kelly TF, Ruoff RS (2000) Strength and breaking mechanism of multiwalled carbon nanotubes under tensile load. *Science* 287:637–640
18. Wu TM, Chen EC, Lin YW, Chiang MF, Chang GY (2008) Preparation and characterization of melt-processed polycarbonate/multiwalled carbon nanotube composites. *Polym Eng Sci* 48:1369–1375
19. Potschke P, Bhattacharyya AR, Janke A (2004) Melt mixing of polycarbonate with multiwalled carbon nanotubes: microscopic studies on the state of dispersion. *Eur Polym J* 40:137–148
20. Maiti S, Shrivastava NK, Suin S, Khatua BB (2013) Formation of interfacial network structure via photo-crosslinking in carbon fiber/epoxy composites. *Express Polym Lett* 7:505–516
21. Monnereau L, Urbanczyk L, Thomassin JM, Alexandre M, Jerome C, Huynen I, Bailly C, Detrembleur C (2014) Supercritical CO₂ and polycarbonate based nanocomposites: a critical issue for foaming. *Polymer* 55:2422–2431
22. Lee SH, Kim JH, Choi SH, Kim SY, Kim KW, Youn JR (2009) Effects of filler geometry on internal structure and physical properties of polycarbonate composites prepared with various carbon fillers. *Polym Int* 58:354–361
23. Chiu FC, Li BH, Jiang JY (2012) Syndiotactic polystyrene/multi-walled carbon nanotube nanocomposites: polymorphism, thermal properties, electrical conductivity, and rheological properties. *Compos A* 43:2230–2240
24. Chiu FC (2014) Comparisons of phase morphology and physical properties of PVDF nanocomposites filled with organoclay and/or multi-walled carbon nanotubes. *Mater Chem Phys* 143:681–692
25. Potschke P, Abdel-Goad M, Pegel S, Jehnichen D, Mark JE, Zhou D, Heinrich G (2009) Comparisons among electrical and rheological properties of melt-mixed composites containing various carbon nanostructures. *J Macromol Sci* 47:12–19
26. Lin B, Sundararaj U, Potschke P (2006) Melt mixing of polycarbonate with multi-walled carbon nanotubes in miniature mixers. *Macromol Mater Eng* 291:227–238
27. Gedler G, Antunes M, Realinho V, Velasco JI (2012) Thermal stability of polycarbonate-graphene nanocomposite foams. *Polym Degrad Stab* 97:1297–1304
28. Fukasawa Y, Chen J, Saito H (2008) A novel nanoporous structure on the surface of bubbles in polycarbonate foams. *J Polym Sci Part B: Polym Phys* 46:843–846
29. Chen L, Ozisik R, Schadler LS (2010) The influence of carbon nanotube aspect ratio on the foam morphology of MWNT/PMMA nanocomposite foams. *Polymer* 51:2368–2375
30. Fan Z, Shu C, Yu Y, Zaporjtchenko V, Faupel F (2006) Vapor-induced crystallization behavior of bisphenol-A polycarbonate. *Polym Eng Sci* 46:729–734
31. Sohn S, Alizadeh A, Marand H (2000) On the multiple melting behavior of bisphenol-A polycarbonate. *Polymer* 41:8879–8886
32. Chiu FC, Kao GF (2012) Polyamide 46/multi-walled carbon nanotube nanocomposites with enhanced thermal, electrical, and mechanical properties. *Compos A* 43:208–218
33. Zhai W, Yu J, Ma W, He J (2007) Cosolvent effect of water in supercritical carbon dioxide facilitating induced crystallization of polycarbonate. *Polym Eng Sci* 47:1338–1343
34. Wunderlich B (1973) *Macromolecular Physics*, vol 1. Academic Press, New York
35. Chiu FC, Fu SW, Chuang WT, Sheu HS (2008) Fabrication and characterization of polyamide 6, 6/organo-montmorillonite nanocomposites with and without a maleated polyolefin elastomer as a toughener. *Polymer* 49:1015–1026